12^{th} International Conference on Fracture Mechanics of Concrete and Concrete Structures
FraMCoS-12
B.L.A. Pichler, Ch. Hellmich, P. Preinstorfer (Eds)

https://doi.org/10.21012/FC12.1227
MS03-2:2

DETERMINATION OF FRACTURE PROCESS ZONE IN HYBRID FIBER REINFORCED ULTRA-HIGH PERFORMANCE CONCRETE USING ACOUSTIC EMISSION ENTROPY

MD ADIL AHMED*, SUDAKSHINA DUTTA†

*Department of Civil Engineering, Indian Institute of Technology
Roorkee, India
e-mail: ma_ahmed@ce.iitr.ac.in

†Department of Civil Engineering, Indian Institute of Technology
Roorkee, India
e-mail: sudakshina@ce.iitr.ac.in

Key words: Fracture process zone, concrete, acoustic emission, entropy, UHPFRC, steel fiber

Abstract. This study investigates the evolution of fracture process zone (FPZ) in ultra-high performance fiber reinforced concrete (UHPFRC) using the acoustic emission (AE) technique. An important factor contributing to the fracture energy in concrete is the nucleation of its FPZ. The examination of FPZ helps in understanding the initiation and propagation of cracks in a material. The influence of different toughening mechanisms within the FPZ helps in predicting the structural integrity and performance of a material when subjected to an external loading. Thus, it is essential to investigate the evolution process of FPZ. In order to determine it, three-point bending tests with monotonic loading are performed on three notched beam specimen groups: ultra-high performance concrete (UHPC) without fibers, UHPFRC with 2% (by volume percentage of concrete, (V_f)) straight micro-fiber, and a hybrid UHPFRC with 1% (V_f) straight micro-fibers and 1% (V_f) straight macro-fibers. Straight micro-steel fibers of 13 mm length and 0.2 mm diameter and straight macro-steel fiber of 26 mm length and 1 mm diameter have been used for the study. An AE parameter based on Shannon's entropy is used to examine the evolution of FPZ. The AE entropy performed more efficiently compared to the other conventional AE parameters on account of it being independent of threshold, and being more sensitive to changes in AE signal irregularities. It is observed that the entropy distribution is greatly influenced by the presence of fibers, indicating a more controlled and distributed cracking process in UHPFRC compared to the brittle behaviour of UHPC without fibers. It is also observed that the FPZ width decreases when straight micro-fibers is partially replaced with straight macro-fibers.

1 INTRODUCTION

Ultra-high performance fiber reinforced concrete (UHPFRC) is an innovative cementitious composite that exhibits extremely high compressive strength, ductility, and durability [1]. With the usage of supplementary cementitious materials such as silica fume, fly ash, and ground granulated blast furnace slag (GGBS), it has also become a more sustainable option in the construction industry compared to conventional concrete [2]. Incorporation of fibers into the UHPFRC mix yields high flexural strength and toughness [3]. It has been observed that using a combination of fibers is more effective in bridging cracks at different scales. The micro-fibers improve the flexural strength and

the macro-fibers contribute to enhance the deformation capability of the structure. Initially, micro-fibers impede the propagation of microcracks followed by arresting macrocrack formation by macro-fibers at a later stage [4, 5]. With the progression of fracture in concrete, an inelastic zone, known as the fracture process zone (FPZ), develops around the crack tip, imparting concrete its nonlinear behavior [6]. Fracture toughness is significantly influenced by the size and development of the FPZ. Therefore, it is important to understand the evolution of FPZ in UHPFRC and the role of fibers in its generation.

Acoustic emission (AE) technique is one of the best methods to study the fracture process in concrete. It has an advantage over other methods due to its ability to record and measure the elastic waves generated during the formation and propagation of cracks [7]. Alam et al. [8] estimated the width and length of the FPZ in concrete beams subjected to three-point loading by determining the region where the cumulative AE event was greater than or equal to 20% of the highest cumulative AE event. The results of the AE analysis showed a good correlation with the DIC observations. Similar results were also reported by Keerthana and Chandra Kishen [9]. This method was based on the work of Otsuka et al. [10], in which they found that the region of AE events that contribute to more than 95% of the total energy represents the FPZ of concrete.

Conventional AE parameters such as AE amplitude, absolute energy, duration, rise time, counts to peak, etc., have been used in the past to study fracture of concrete. These parameters have their own limitations. AE entropy, initially introduced by Claude E. Shannon, seems to overcome these limitations. It was first introduced in 1948 by the name of information entropy [11]. Santo et al. [12] observed that with increasing threshold value the different AE parameters, namely, AE energy, count, duration, and rise time, were reduced. Only AE entropy and amplitude were found to be independent of threshold; but unlike amplitude, AE entropy carried the necessary information to predict the waveform characteristics. Change in hit definition time was also found to affect all the AE parameters except entropy. Using AE entropy, Kahirdeh et al. [13] could identify three distinct stages of damage in composites. Ahmed and Dutta [14] used AE entropy to differentiate the different damages stages, i.e., fiber-matrix debonding, friction, and fiber rupture during the pull-out process of a steel fibers from an UHPC matrix. A strong correlation was also observed between the evolution of AE count and entropy [15].

The prediction of FPZ in UHPFRC using AE entropy is sparse. Therefore, the aim of this investigation is to study the size and evolution of FPZ in UHPC and hybrid UHPFRC using AE entropy based on Shannon's entropy.

2 METHODOLOGY

2.1 Materials and specimen preparation

Ordinary Portland cement of 43 grade, silica fume, and GGBS are used as binders. River sand with grain size between 0.15 and 4.75 mm is used as fine aggregate. To improve the workability of the mix, a polycarbolxylate-based superplasticizer is used. The mix proportions used in this study are summarized in Table 1. Pan mixer has been used to prepare the mixes. The samples are cured in hot water at 90^0C for 2 days before being transferred to normal water. The 28 days compressive strength performed on 100 mm cubes is 125 MPa.

Table 1: Mix Proportion

Unit Weight (kg/m^3)						
Cement	Silica Fume	GGBS	Quartz Powder	Sand	Water	Superplasticizer
716.8	102.4	204.8	77	1024	195	14

In order to investigate the influence of fibers on the development of the fracture process zone, straight micro and macro-steel fibers are included. The properties of the steel fibers are given in Table 2. Three groups of notched beam specimens of dimensions 200 x 200 x 650 mm are cast according to ASTM C1856 with a notch-to-depth ratio of 0.2. They are - Control beams (C) cast without fibers, UHPFRC (s2)

with 2% (V_f) straight micro-fiber, and a hybrid UHPFRC (Hs1S1) with 1% (V_f) straight micro-fibers and 1% (V_f) straight macro-fibers.

Beams with predefined notches are selected in this study so as to localize the damage at the notch-plane. This prevents the inelastic deformation of the remaining portion of the beam, and ensures the major part of the energy to be directly attributed to the fracture along the notch-plane [16]. This controlled damage process is not possible in unnotched specimen where cracks may develop in different zones across the specimen, thus making characterization of the FPZ more challenging.

Table 2: Details of Steel Fibers

Straight fiber type	Diameter (mm)	Length (mm)	Tensile Strength (MPa)
Micro	0.2	13	2800
Macro	1	26	1200

2.2 Experimental set-up

The beams have been tested in a closed loop servo-controlled universal testing machine of 300 kN capacity. A displacement rate of 0.2 mm/min has been used. AE monitoring has been performed using a 16-bit AE data acquisition system. Six piezoelectric sensors (MISTRAS R6I) with built-in preamplifiers of 40 db gain have been used to locate the AE sources. The threshold is set at 40 dB to filter out background noise.

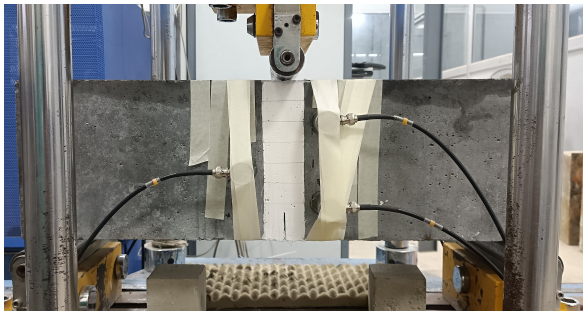

Figure 1: Experimental set-up

2.3 DETERMINATION OF ENTROPY

AE waves generated during the initiation and propagation of cracks in a beam subjected to flexural loading will have a unique disorder in its waveform. This can be quantified to identify the different damage stages. One way of achieving it is by obtaining the probability distribution of the waveform's discrete voltage value, termed as information entropy [12].

The information entropy or Shannon's entropy is given by:

$$H = -c\sum_{i=1}^{n} p(x_i) * log(p(x_i)) \quad (1)$$

Where, $x_1, x_2, x_3, ...x_n$ are a given random sequence. $p(x_i)$ is its associated probability mass. H is the non-negative Shannon's entropy. C is an arbitrary positive constant being equal to 1/log(2). The unit of its measurement is in bits.

3 RESULTS AND DISCUSSIONS

3.1 Flexural behavior

The flexural performance of UHPC, UHPFRC, and hybrid UHPFRC are shown in Figure 2.

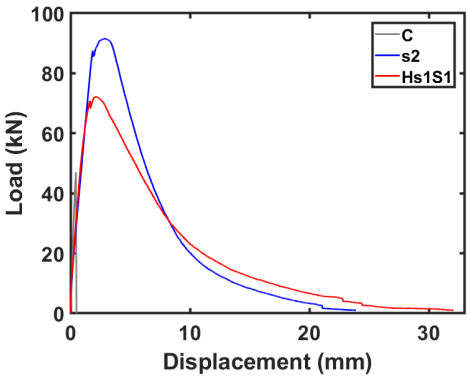

Figure 2: Average Load-displacement curve for control, s2, and Hs1S1 specimen.

As evident, the UHPC sample without fiber behaved almost linearly up to the peak-load where it underwent brittle failure with complete separation of the sample in two halves. Whereas, the UHPFRC samples, irrespective of the type of fiber, experienced a tri-linear variation with the formation of multiple cracks during the load bearing process of the beam [17]. In UHPFRC specimen, initially the load increases linearly till the occurrence of the first

crack. Post that stage it increases non-linearly till it reaches the peak load, beyond which the load decreases. Both the specimen group s2, and Hs1S1 showed deflection-hardening behavior. This happens in specimens where $f_{LOP}<f_{MOR}$ due to the crack arresting capacity of the fibers [4] (Table 3). Here, f_{LOP} represents the first and f_{MOR} represents the post-cracking flexural strengths, respectively. Straight micro-fibers are efficient in restricting the formation of microcracks. Hence, the specimen - s2 shows the highest peak load and f_{MOR}. The hybrid fiber UHPFRC specimen, even though having a lower peak load, sustains the load for a larger displacement value due to the presence of longer straight steel fiber that prevents the propagation of macroscopic cracks. These also makes its fracture energy almost similar to the micro-fiber UHPFRC specimen as shown in Table 3.

Table 3: Flexural performance of UHPC and UHPFRC specimens

Group	Peak load (kN)	Max displacement (mm)	f_{LOP} (MPa)	f_{MOR} (MPa)	Fracture energy (N/mm)
C	47.09	0.51	8.28	8.28	0.39
s2	91.64	23.88	15.39	16.11	20.27
Hs1S1	72.32	32.04	12.40	12.71	19.92

3.2 Damage stage identification using AE parameters

Figure 3, Figure 4, and Figure 5, shows the AE parameter - AE entropy, AE amplitude, and AE absolute energy (called as energy in this study), corresponding to each event recorded during the flexural tests on control, UHPFRC, and hybrid UHPFRC sample, respectively. Even though the results obtained for control specimen with respect to the AE parameters is similar, owing to the damage being mainly dominated by matrix failure, a noticeable difference is observed in UHPFRC specimens. There is a high rate of AE activity recorded in the initial stage of loading till the peak load due to the formation and initiation of multiple microcracks in the concrete. At the same instance, the micro-fibers are also restricting the crack initiations. As the load approaches it peak value, the fiber pull-out resistance dominates at the crack surface [18]. Post-peak load, the microcracks coalesces into macrocracks and the load starts decreasing.

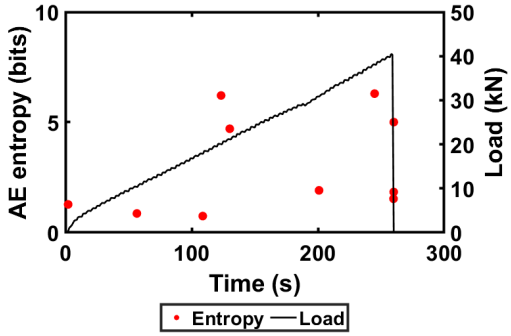

(a) Load-time-AE entropy

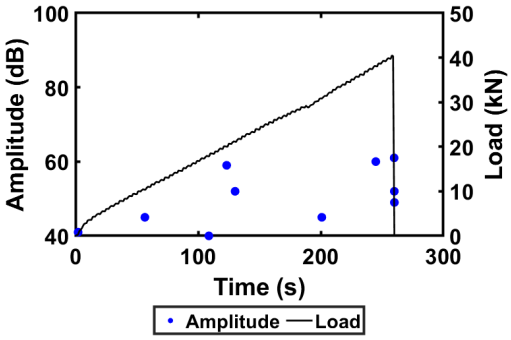

(b) Load-time-AE amplitude

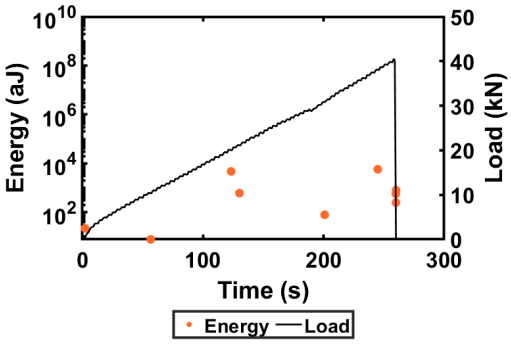

(c) Load-time-AE energy

Figure 3: Correlation of load vs. time curve with AE parameters for control specimen.

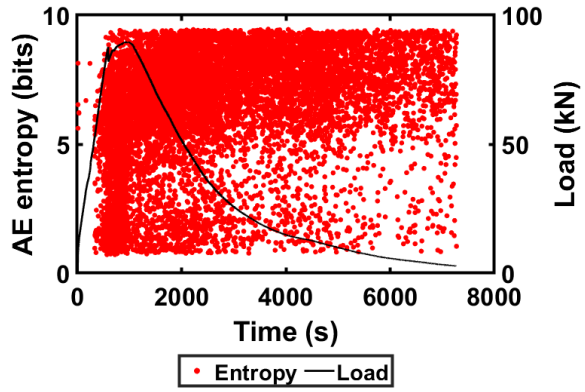

(a) Load-time-AE entropy

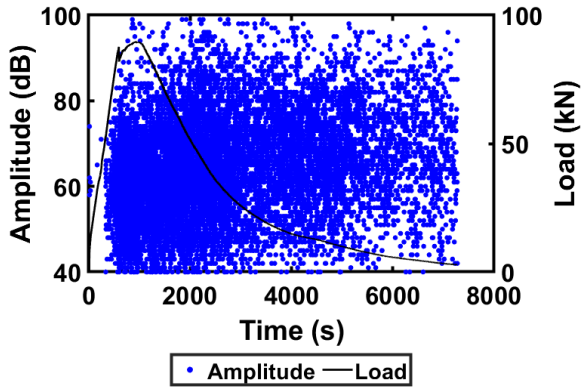

(b) Load-time-AE amplitude

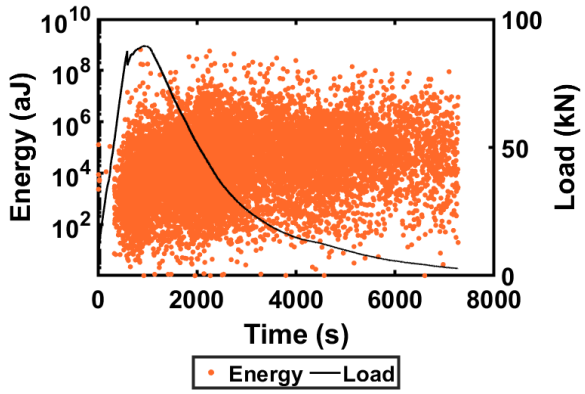

(c) Load-time-AE energy

Figure 4: Correlation of load vs. time curve with AE parameters for s2 specimen.

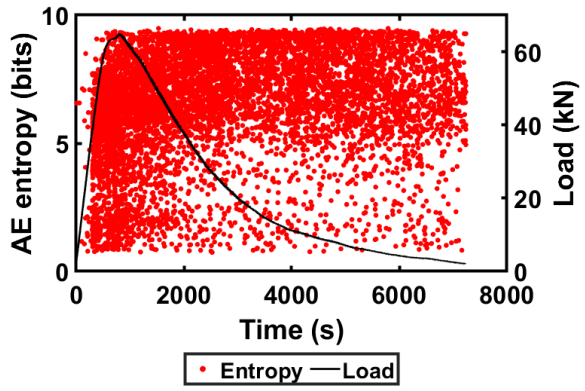

(a) Load-time-AE entropy

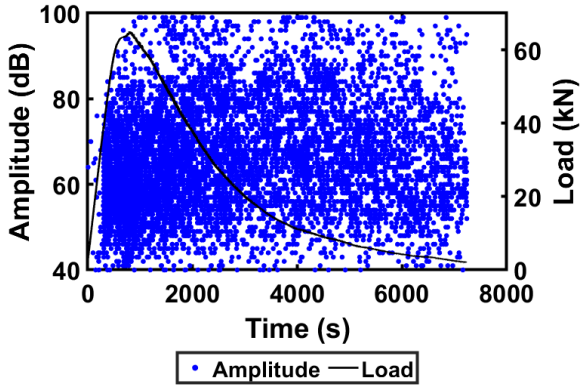

(b) Load-time-AE amplitude

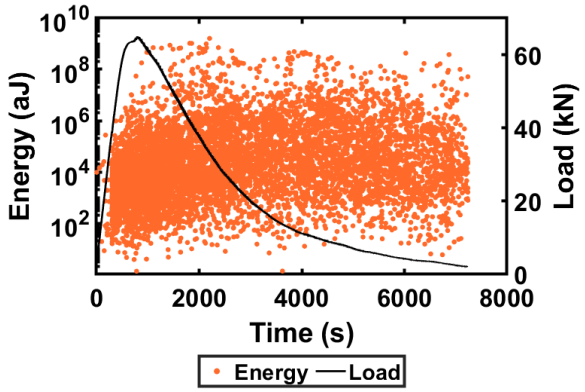

(c) Load-time-AE energy

Figure 5: Correlation of load vs. time curve with AE parameters for Hs1S1 specimen.

The AE entropy depicts these stages efficiently as evident in Figure 4a, and Figure 5a. Most of the AE entropy value remains above 6 bits depicting this stage to be dominated by partial and complete debonding between fiber-matrix interface, followed by initiation of pull-out of fibers from the matrix as shown in the authors' previous work [14]. However, such distinctions are not observed in other AE parameters for both types of UHPFRC specimens. Thus, further studies on FPZ have been done using AE entropy because of its effectiveness in identifying the damage stages.

3.3 Identification of FPZ using AE entropy

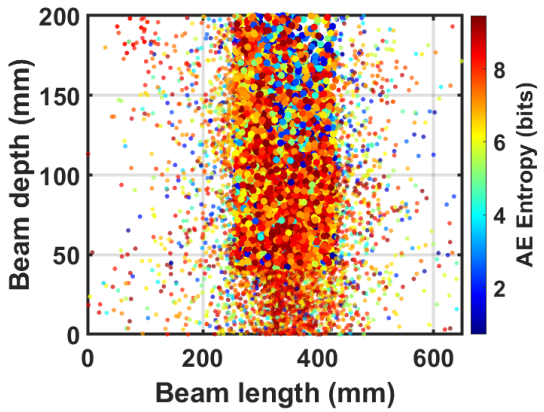

(a) Localization of AE entropy

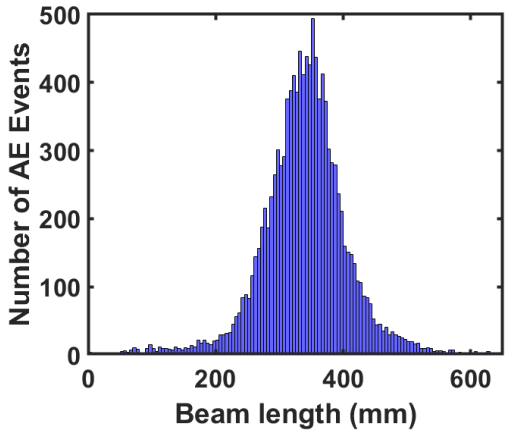

(b) Cumulative AE event at each location along the beam length for FPZ width calculation

Figure 6: FPZ width from AE analysis for s2 specimen.

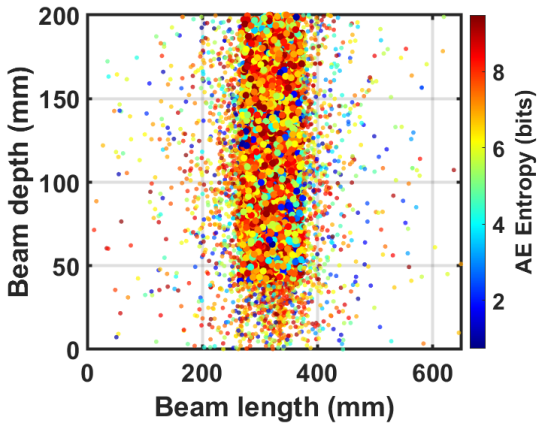

(a) Localization of AE entropy

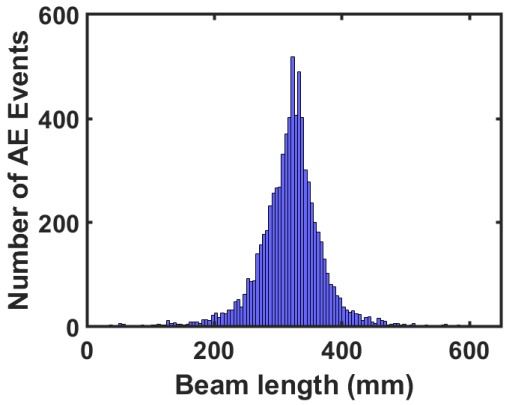

(b) Cumulative AE event at each location along the beam length for FPZ width calculation

Figure 7: FPZ width from AE analysis for Hs1S1 specimen.

It has been reported in the past that the percentage of total energy of AE events that is greater than 95% of the total energy of the entire events belongs to the fracture process zone [10]. For our present study, we have found those range of entropy values whose corresponding total energy are more than 95% of the total AE energy. This range is found to be between 6-9.5 bits. This also agrees with the result of the previous section where entropy higher than 6 bits depicted the dominant damage stages. Moreover, cumulative AE events has also been used in the past to quantify the FPZ width [8, 9]. In this method, cumulative AE events are recorded at each location along the length of the beam.

Those events which are higher than 20% of the maximum cumulative event value is said to be coming from the FPZ region. This region, with large number of events, depicts the localization of microcracks. Using both the above mentioned approach (refer Figure 6, and Figure 7), the FPZ width obtained for s2, and Hs1S1 specimen are 175 mm, and 110 mm, respectively. The UHPFRC sample having more percentage of straight micro-fiber has a larger FPZ width due to the generation of more AE activity coming from the toughening mechanism inside the FPZ as compared to the hybrid UHPFRC specimen.

Further, from authors' previous work [14], it has been identified that the events with entropy in the range of 7.5-9.5 bits originate around the complete debonding of fiber-matrix interface. Once debonded, the fibers are pulled out from the matrix and formation of macrocracks begins. This information can be used to identify the fracture core zone (FCZ) where the developement of macocracks takes place [10]. Thus, entropy, unlike other localization methods, can also be used to identify FCZ as well.

3.4 FPZ evolution

The formation and propagation of FPZ can be studied using AE entropy, that belongs to the 95% energy group, by noting their appearance at various stages. Figure 8 and Figure 9 shows the different flexural damage stages in both the UHPFRC samples along with the damage progression. Point A depicts the initiation stage of microcrack. From point A to B, depicts the evolution phase of macrocrack, and from B to point C represents the propagation stage of the main macrocrack. As can be seen in both Figure 8b and Figure 9b, as the load approaches point A, few AE entropy of lower magnitude are generated due to the formation of microcracks. Some of them have occurred near the top load due to the pressing of the loading roller against the top surface of the beam. When the load approaches point B (i.e., peak load), AE events with higher entropy values are generated near the notch (Figure 8c and Figure 9c). This is the region of the beam which is the most stressed and leads to the resisting action of the fibers on the microcrack initiation. Beyond point B till point C, microcracks coalesces to form macrocracks, along with the occurence of fiber-matrix interface debonding and fiber pull-out processes. This generates a large number of AE entropy in the fracture process zone as shown in Figure 8d and Figure 9d.

4 Conclusion

In this study, AE entropy has been used to identify the damage stages in UHPC and UHPFRC beams with single type of straight microfibers and a hybrid combination of straight micro and macro-steel fibers subjected to flexural loading. AE entropy proved to be more efficient than other AE parameters - amplitude and energy, in distinguishing the crack propagation stages because of its ability to capture the disorder associated with each AE waveform. The AE entropy value above 6 bits mostly originated from the fracture process zone as it contributed to more than 95% of the total AE energy. This observation was used to determine the FPZ width from the entropy localization map. It was observed that the width of the FPZ decreased when the micro-fibers were replaced with macro-fibers. The macro-fibers in the hybrid UHPFRC mix arrested the propagation of cracks and delayed the macrocrack formation process. Further, the propagation of FPZ at three different damage stages was also studied. In the microcrack initiation stage, few microcracks are formed. In the evolution of macrocrack stage the weak microcracks begin to merge into macrocracks, and finally in the macrocrack propagation phase the main macrocrack propagates from bottom to the top of the specimen. At present, the analysis has been carried out in time domain solely. It will be an interesting aspect to carry out a frequency domain analysis to correlate the different damage mechanisms with the frequencies of the AE signals in future.

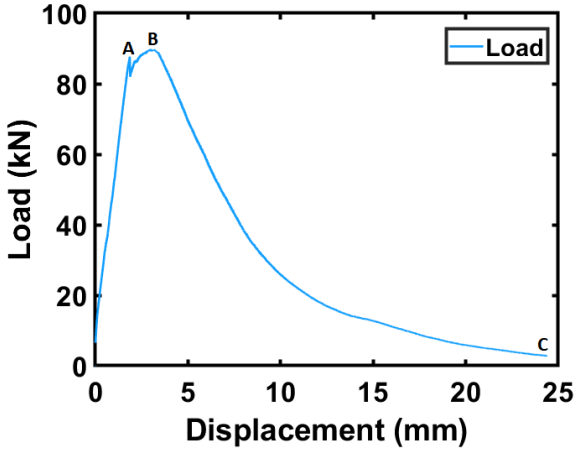

(a) Load-displacement curve for s2 specimen

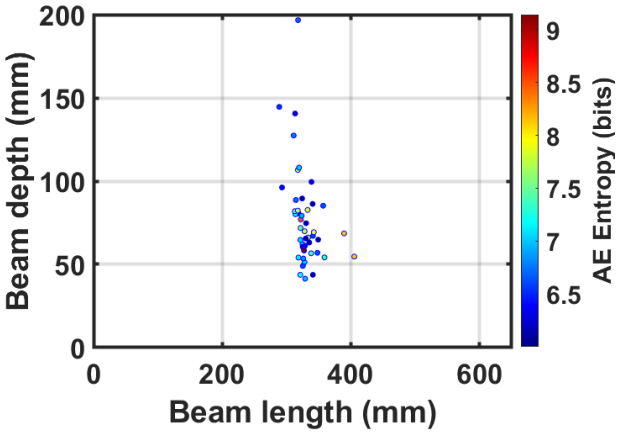

(b) AE entropy at point A

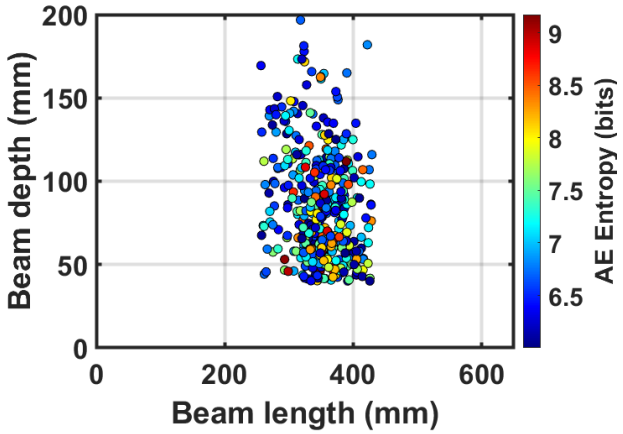

(c) AE entropy at point B

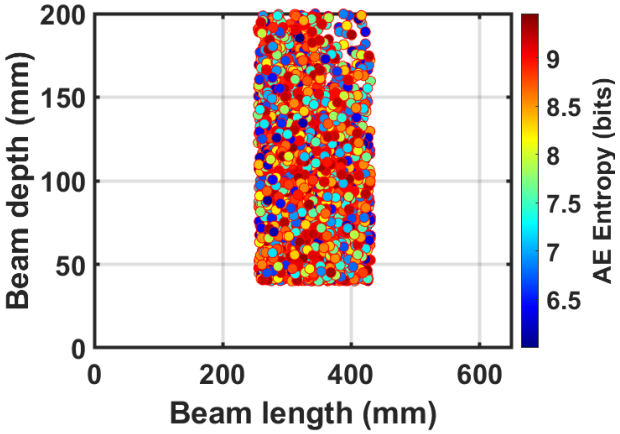

(d) AE entropy at point C

Figure 8: Evolution of micro and macro cracks in UHPFRC beam (s2) specimen. (a) Load-displacement curve, (b) AE entropy at point A, (c) AE entropy at point B, (d) AE entropy at point C.

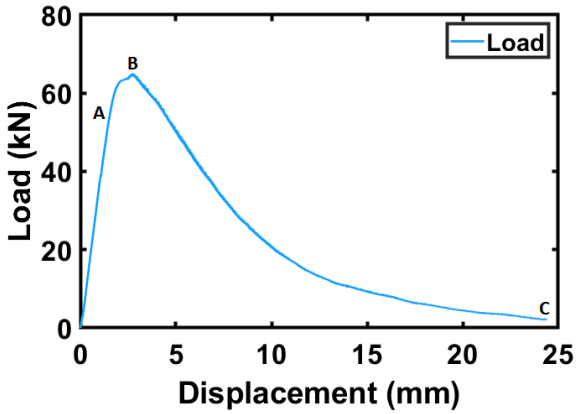

(a) Load-displacement curve for Hs1S1 specimen

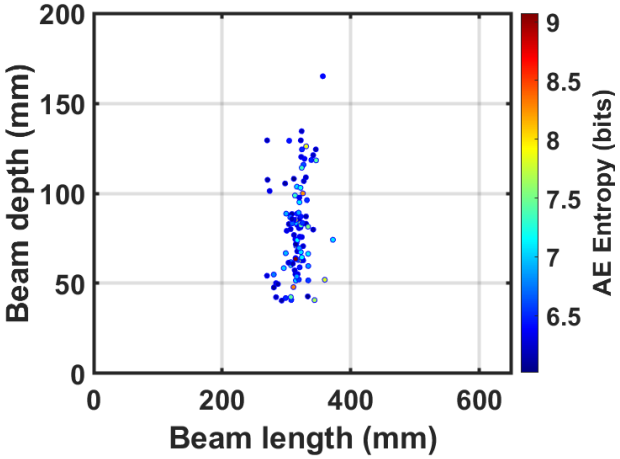

(b) AE entropy at point A

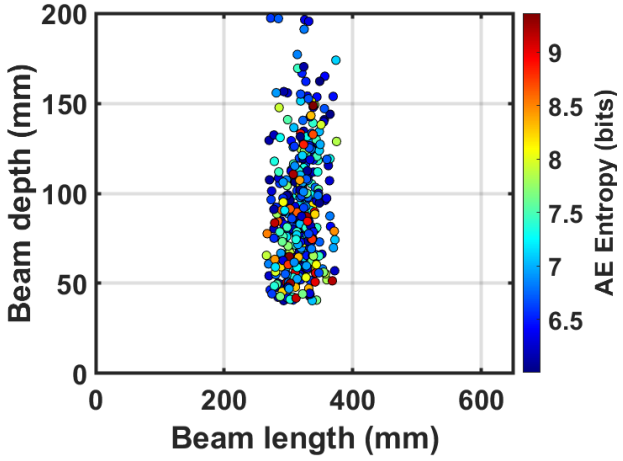

(c) AE entropy at point B

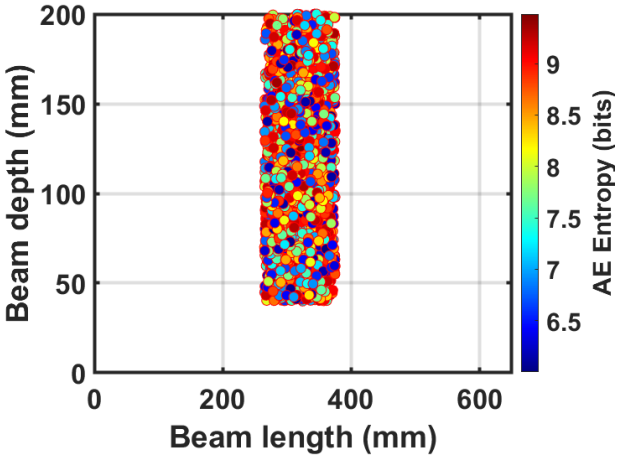

(d) AE entropy at point C

Figure 9: Evolution of micro and macro cracks in UHPFRC beam (Hs1S1) specimen. (a) Load-displacement curve, (b) AE entropy at point A, (c) AE entropy at point B, (d) AE entropy at point C.

REFERENCES

[1] MA Bajaber and IY Hakeem. Uhpc evolution, development, and utilization in construction: A review. *Journal of Materials Research and Technology*, 10:1058–1074, 2021.

[2] Mugahed Amran, G Murali, Natt Makul, WC Tang, and Ayed Eid Alluqmani. Sustainable development of eco-friendly ultra-high performance concrete (uhpc): Cost, carbon emission, and structural ductility. *Construction and Building Materials*, 398:132477, 2023.

[3] Weina Meng and Kamal H Khayat. Effect of hybrid fibers on fresh properties, mechanical properties, and autogenous shrinkage of cost-effective uhpc. *Journal of Materials in Civil Engineering*, 30(4):04018030, 2018.

[4] Yanfei Niu, Jiangxiong Wei, and Chujie Jiao. Crack propagation behavior of ultra-high-performance concrete (uhpc) reinforced with hybrid steel fibers under flexural loading. *Construction and Building Materials*, 294:123510, 2021.

[5] Zemei Wu, Caijun Shi, Wen He, and Dehui Wang. Static and dynamic compressive properties of ultra-high performance concrete (uhpc) with hybrid steel fiber reinforcements. *Cement and concrete composites*, 79:148–157, 2017.

[6] Jacqueline Saliba, Ahmed Loukili, Jean-Pierre Regoin, David Grégoire, Laura Verdon, and Gilles Pijaudier-Cabot. Experimental analysis of crack evolution in concrete by the acoustic emission technique. *Frattura ed Integrità Strutturale*, 9(34), 2015.

[7] Kentaro Ohno, Kimitaka Uji, Atsushi Ueno, and Masayasu Ohtsu. Fracture process zone in notched concrete beam under three-point bending by acoustic emission. *Construction and building materials*, 67:139–145, 2014.

[8] Syed Yasir Alam, Jacqueline Saliba, and Ahmed Loukili. Fracture examination in concrete through combined digital image correlation and acoustic emission techniques. *Construction and Building Materials*, 69:232–242, 2014.

[9] K Keerthana and JM Chandra Kishen. Micromechanics of fracture and failure in concrete under monotonic and fatigue loadings. *Mechanics of materials*, 148:103490, 2020.

[10] Koji Otsuka and Hidehumi Date. Fracture process zone in concrete tension specimen. *Engineering fracture mechanics*, 65(2-3):111–131, 2000.

[11] Claude Elwood Shannon. A mathematical theory of communication. *The Bell system technical journal*, 27(3):379–423, 1948.

[12] Farhan Tanvir Santo, Tariq Pervez Sattar, and Graham Edwards. Validation of acoustic emission waveform entropy as a damage identification feature. *Applied Sciences*, 9(19):4070, 2019.

[13] Ali Kahirdeh. *Energy dissipation and entropy generation during the fatigue degradation: Application to health monitoring of composites*. Louisiana State University and Agricultural & Mechanical College, 2014.

[14] Md Adil Ahmed and Sudakshina Dutta. Study of damage mechanisms in ultra high performance concrete using acoustic emission technique.

[15] Mehdi Amiri, Mohammad Modarres, and Enrique López Droguett. Ae entropy for detection of fatigue crack initiation and growth. In *2015 IEEE Conference on Prognostics and Health Management (PHM)*, pages 1–8. IEEE, 2015.

[16] Vellore S Gopalaratnam and Ravindra Gettu. On the characterization of flexural toughness in fiber reinforced concretes. *Cement and concrete composites*, 17(3):239–254, 1995.

[17] Francesco Bencardino, L Rizzuti, G Spadea, and RN Swamy. Experimental evaluation of fiber reinforced concrete fracture properties. *Composites Part B: Engineering*, 41(1):17–24, 2010.

[18] Doo-Yeol Yoo, Min Jae Kim, Sung-Wook Kim, and Jung-Jun Park. Development of cost effective ultra-high-performance fiber-reinforced concrete using single and hybrid steel fibers. *Construction and Building Materials*, 150:383–394, 2017.